1   **Structure-function relation of the developing calyx of Held synapse *in vivo***

2

3   **Running title:** Strength-size relation of the calyx of Held

4   **Martijn C. Sierksma[1,3], Johan A. Slotman[2], Adriaan B. Houtsmuller[2] and J. Gerard G. Borst[1]**

5   [1]Department of Neuroscience or [2]Department of Pathology – Optical Imaging Centre, Erasmus

6   MC, University Medical Center Rotterdam, 3000 CA, Rotterdam, The Netherlands.

7   [3]Sorbonne Université, Inserm, CNRS, Institut de la Vision, 17 Rue Moreau, F-75012 Paris,

8   France.

9   Correspondence to g.borst@erasmusmc.nl

10

11   **Table of contents category:** Neuroscience, Research paper

12   **Key words**: Synaptic transmission/In vivo electrophysiology/auditory development

Key points summary

1. During development the giant, auditory calyx of Held forms a one-to-one connection with a principal neuron of the medial nucleus of the trapezoid body.

2. While anatomical studies described that most of the target cells are temporarily contacted by multiple calyces, multi-calyceal innervation was only sporadically observed in *in vivo* recordings, suggesting a structure-function discrepancy.

3. We correlated synaptic strength of inputs, identified in *in vivo* recordings, with post hoc labeling of the recorded neuron and synaptic terminals containing vesicular glutamate transporters (VGluT).

4. During development only one input increased to the level of the calyx of Held synapse, and its strength correlated with the large VGluT cluster contacting the postsynaptic soma.

5. As neither competing strong inputs nor multiple large VGluT clusters on a single cell were observed, our findings did not indicate a structure-function discrepancy.

Abstract

In adult rodents, a principal neuron in the medial nucleus of the trapezoid (MNTB) is generally contacted by a single, giant axosomatic terminal called the calyx of Held. How this one-on-one relation is established is still unknown, but anatomical evidence suggests that during development principal neurons are innervated by multiple calyces, which may indicate calyceal competition. However, *in vivo* electrophysiological recordings from principal neurons indicated that only a single strong synaptic connection forms per cell. To test whether a mismatch exists between synaptic strength and terminal size, we compared the strength of synaptic inputs with the morphology of the synaptic terminals. *In vivo* whole-cell recordings of the MNTB neurons from newborn Wistar rats of either sex were made while stimulating their afferent

2

41   axons, allowing us to identify multiple inputs. The strength of the strongest input increased to

42   calyceal levels in a few days across cells, while the strength of the second strongest input was

43   stable. The recorded cells were subsequently immunolabeled for vesicular glutamate

44   transporters (VGluT) to reveal axosomatic terminals with structured-illumination microscopy.

45   Synaptic strength of the strongest input was correlated with the contact area of the largest

46   VGluT cluster at the soma (r = 0.8), and no indication of a mismatch between structure and

47   strength was observed. Together, our data agree with a developmental scheme in which one

48   input strengthens and becomes the calyx of Held, but not with multi-calyceal competition.

49

Introduction

50

51 Synapses are specialized structures that allow presynaptic signals to be transmitted to the

52 postsynaptic side. Most central synapses use neurotransmitters for signaling, and these

53 chemical synapses come in a large variety of sizes and shapes. While most synapses have a

54 diameter of about one μm and are formed on a dendrite, some synapses can be >10 μm, and

55 encompass >100 release sites (Walmsley *et al.*, 1998; Atwood & Karunanithi, 2002;

56 Rollenhagen & Lübke, 2006). These large synapses have facilitated the study of the biophysical

57 properties of synapses. A prime example is the calyx of Held synapse in the auditory

58 brainstem. The presynaptic calyx spans ~20 μm, large enough to be accessible for patch-clamp

59 electrophysiology (Forsythe, 1994; Borst *et al.*, 1995) and to allow simultaneous recording of

60 the calyx and its postsynaptic target (Borst *et al.*, 1995), a glycinergic neuron in the medial

61 nucleus of the trapezoid body (MNTB). Owing to the presence of hundreds of active zones

62 (Sätzler *et al.*, 2002; Taschenberger *et al.*, 2002; Dondzillo *et al.*, 2010), the calyx of Held can

63 rapidly trigger postsynaptic action potentials (APs), thus functioning as a fast, high-fidelity,

64 inverting relay in the auditory brainstem (Borst & Soria van Hoeve, 2012).

65 During its development, the calyx of Held synapse grows from an axon of a globular bushy cell

66 (GBC) that initially forms small boutons. In rodents these contacts already appear before birth

67 (Kandler & Friauf, 1993; Hoffpauir *et al.*, 2006; Rodríguez-Contreras *et al.*, 2008; Hoffpauir *et*

68 *al.*, 2010; Holcomb *et al.*, 2013). Although the innervation initially is highly divergent,

69 eventually a GBC will give rise to only one or a few calyces, and most adult principal neurons

70 are innervated by a single calyx of Held (Held, 1893; Morest, 1968; Kuwabara *et al.*, 1991;

71 Kandler & Friauf, 1993; Rodríguez-Contreras *et al.*, 2006). The developmental mechanisms that

72 ensure the transition to the one-on-one innervation are largely unclear (Yu & Goodrich, 2014).

73 This transition happens between the second and the fifth postnatal day (P2-5). At P5 the

74 strength of one input overshadows the other ones (Chuhma & Ohmori, 1998; Hoffpauir *et al.*,

75 2006; Hoffpauir *et al.*, 2010; Sierksma *et al.*, 2016), and one of the terminals has expanded

4

76   over the soma of the neuron (Hoffpauir *et al.*, 2006; Holcomb *et al.*, 2013). From these studies

77   it was suggested that half of the MNTB neurons are contacted by multiple calyces at this age

78   range (Hoffpauir *et al.*, 2010; Holcomb *et al.*, 2013; Milinkeviciute *et al.*, 2019), in agreement

79   with observations from mouse slice recordings (Bergsman *et al.*, 2004; Hoffpauir *et al.*, 2010;

80   Xiao *et al.*, 2013). Note that multi-calyceal innervation is defined here as an MNTB neuron that

81   is innervated by more than one calyx of Held, and not as an MNTB neuron that is innervated by

82   multiple calycigenic axons.

83   The developmental changes that underlie the formation of the calyx of Held synapse may

84   involve activity-dependent processes. In newborn, pre-hearing rodents, spontaneous activity,

85   arising in the cochlea (Tritsch *et al.*, 2010), propagates across the developing auditory

86   brainstem (Sonntag *et al.*, 2009; Tritsch *et al.*, 2010; Crins *et al.*, 2011; Sierksma *et al.*, 2016).

87   The correlated, bursting activity of presynaptic terminals (Sierksma & Borst, 2017) causes

88   plateau-like depolarizations in the postsynaptic cell (Sierksma *et al.*, 2016) and bursting activity

89   (Tritsch *et al.*, 2010; Crins *et al.*, 2011; Clause *et al.*, 2014) which may induce synaptic plasticity.

90   The presence of multiple calyces contacting the same target neuron would suggest that the

91   formation of a one-to-one connection involves some form of competition during which one

92   calyx rapidly expands and increases in strength, whereas the other contacts retract and

93   decrease in strength. However, in the rat, *in vivo* physiological evidence for calyceal

94   competition was observed in only very few cases (Sierksma *et al.*, 2016).

95   These findings may indicate a discrepancy between terminal size and synaptic strength. To test

96   this possibility, one needs to correlate synaptic structures with synaptic strength. Serial

97   sectioning of tissue combined with EM offers the possibility of fully reconstructing every

98   synapse in a restricted volume (Denk & Horstmann, 2004; Hoffpauir *et al.*, 2006; Holcomb *et*

99   *al.*, 2013), and allows the reconstruction of entire calyces (Sätzler *et al.*, 2002; Holcomb *et al.*,

100 2013; Qiu *et al.*, 2015). However, it does not offer a direct estimate of synaptic strength.

5

101   Whereas slice electrophysiology has the advantage of allowing simultaneous recordings of pre-

102   and postsynaptic structures (Borst *et al.*, 1995; Rodríguez-Contreras *et al.*, 2008), there is the

103   uncertainty associated with possible cutting of inputs during slice preparation. Immunolabeling

104   of vesicular glutamate transporters (VGluT) localizes synapses in the MNTB (Rodríguez-

105   Contreras *et al.*, 2006; Rodríguez-Contreras *et al.*, 2008; Soria Van Hoeve & Borst, 2010;

106   Milinkeviciute *et al.*, 2019). Parvalbumin may identify calyces, but not at the youngest ages

107   (Lohmann & Friauf, 1996, but see Felmy & Schneggenburger, 2004), and its presence does not

108   indicate whether the calyx is release-competent. As Piccolo, an active zone protein (Südhof,

109   2012; Gundelfinger *et al.*, 2016), is present in young calyces (Dondzillo *et al.*, 2010), the

110   combination of VGluT and Piccolo may indicate synaptic connectivity in the MNTB. How VGluT

111   relates to synaptic strength is still unclear.

112   Here, we combined VGluT immunolabeling with *in vivo* whole-cell recordings during which we

113   recorded the inputs that are regularly active (Lorteije *et al.*, 2009; Sierksma *et al.*, 2016). We

114   applied electrical stimulation of the afferent axons to further identify the developing inputs.

115   The recorded cells were subsequently immunolabeled for VGluT and Piccolo, allowing a direct

116   comparison between synapse strength and structure for the developing calyx of Held synapse.

6

117   **Methods**

118   ***Ethical approval***

119   All procedures conformed to the European Directive 2010/63/EU and were approved by the

120   local animal ethics committee (EDC, project no. 115-14-11). Timed-pregnant Wistar rats (WU)

121   were purchased from Charles River and housed within the Erasmus animal facility (EDC). The

122   day of birth or finding the litter was taken as postnatal day (P)0. The dams had *ad libitum*

123   access to food and water, and additional bedding and shelter material was provided for nest

124   building. Wistar pups of undetermined sex were taken from the nest on the day of the

125   experiment. The authors understand the ethical principles under which the journal operates

126   and confirm that their work complies with the animal ethics checklist provided by the editorial

127   board.

128   ***Surgery***

129   The pup was anesthetized with isoflurane administered together with medical oxygen.

130   Anesthesia depth was checked by the paw pinch prior to the surgery. We used a ventral

131   approach to gain access to the auditory brainstem, as described previously (Rodríguez-

132   Contreras *et al.*, 2008; Sierksma *et al.*, 2016). After recording the animal was deeply

133   anesthetized and perfused with 6-10 mL of cold saline (0.9% NaCl, w/v), followed by 8-10 mL

134   of 4% of paraformaldehyde (PFA, w/v) dissolved in 0.12 M phosphate-buffer (PB, pH 7.2-7.4).

135   ***In vivo electrophysiology***

136   First, we searched for bursting activity with a glass electrode to find the presumed location of

137   the MNTB. When bursting activity was found, the search pipette was retracted and a bipolar

138   stimulation electrode (MicroProbes for Life Science, PI2ST30.1H10) was placed contralateral

139   from the recorded MNTB, straddling the trapezoid body, as described by Crins *et al.* (2011).

140   Successful placement was assessed by measuring the stimulation current threshold and the

141   presence of a field potential.

142   Whole-cell recordings with biocytin (2 mg/mL) in the pipette solution were made from

143   principal cells; to be confident that the recording was obtained from the same neuron as the

144   one that was recovered with immunolabeling, we made whole-cell recordings from a single

145   principal neuron per animal. Whenever a glia cell or non-principal cell was encountered, the

146   pipette was retracted and a new pipette was used. Membrane potentials were compensated

147   prior to the recordings for a liquid junction potential of -11 mV. Drift in membrane potential

148   was <5 mV and remained uncorrected. Recordings were made with a MultiClamp 700B in

149   current-clamp mode, with bridge balance set in the range of 20-70 MΩ and pipette

150   capacitance compensation ~4-6 pF. Signals were low-pass filtered with a 4-pole Bessel filter at

151   10 kHz and digitized by a DigiData 1440A (Molecular Devices Co.) at 25 kHz. Acquisition was

152   done with Clampex 10.2 running on a Windows XP computer.

153   Stimulation intensities were manually adjusted during the experiments. First, we quickly

154   assessed at which stimulation levels new excitatory postsynaptic potentials (EPSPs) were

155   recruited, and at which polarity most inputs could be discerned. Then, stimulation intensity

156   was lowered to the activation threshold of the first input, and step-wise increased over time.

157   In some experiments the stimulation intensity was also stepwise reduced, and then the data

158   were pooled. For every stimulation strength >30 sweeps were collected at 2 Hz. Stimulation

159   current was typically below 0.4 mA to prevent damage to the axons; at high stimulation

160   currents (0.3 mA or higher) antidromic APs with latencies <1 ms were often elicited in the

161   principal neuron. This could still happen even though we used bipolar stimulation electrodes,

162   placed on the contralateral side from the recorded neuron. Preferably, the stimulation

163   electrode would be placed at the midline, where all calycigenic axons converge ventrally.

164   However, to avoid direct postsynaptic activation we placed the stimulation electrode more

165   laterally. This location may have led to preferential activation of the axon bundles that run

166   ventrally from the other MNTB (Kandler & Friauf, 1993).

8

167   Labeling calyces by *in vivo* whole-calyx recordings or electroporation was performed as

168   described previously (Sierksma & Borst, 2017).

169   ***Antibodies***

170   The following primary antibodies were used: rabbit polyclonal anti-Piccolo (Synaptic Systems

171   142003, RRID: AB_2160182; 1:1000), guinea-pig polyclonal anti-vesicular glutamate

172   transporter 1 (Millipore AB5905, RRID: AB_2301751; 1:3000) and 2 (Millipore AB2251, RRID:

173   AB_1587626; 1:3000). Secondary antibodies Alexa Fluor 488 against rabbit and Alexa Fluor 645

174   against guinea pig were obtained from Jackson (1:200 or 1:400). Streptavidin-Alexa Fluor 594

175   conjugate (1:200) was obtained from Thermo Fisher Scientific. Throughout, VGluT labeling

176   refers to both VGluT1 and VGluT2.

177   ***Immunolabeling procedure***

178   Immunolabeling procedure was based on the free-floating method. After perfusion the brain

179   was carefully removed from the skull, and post-fixed overnight at 4 °C. Then, it was left

180   overnight in 10% (w/v) sucrose in 0.1 M PB, embedded in 10% (w/v) gelatin and 10% (w/v)

181   sucrose, and again fixed overnight at 4 °C in 30% (w/v) sucrose and 10% (w/v) formaldehyde.

182   The brain was cryoprotected with 30% (w/v) sucrose solution in 0.1 M PB for >24 hr at 4 °C.

183   Coronal slices (40 µm) were made on a freezing microtome, and were collected in 0.1 M PB.

184   The sections were heated for 3 hr to 80 °C in 10 mM sodium citrate (pH 6 at RT), washed four

185   times for 10 min with 0.9% (w/v) NaCl in 0.05 M PB (PBS). Then, the sections were pre-

186   absorbed for 1 hr at RT with 10% (v/v) normal horse serum and 10% (v/v) Triton X-100 in PBS

187   followed by 36-48 hr incubation under gentle agitation at 4 °C with primary antibody solution

188   containing 2% (v/v) normal horse serum, 0.4% (v/v) Triton X-100 and the primary antibodies.

189   The slices were washed four times for 10 min in PBS at RT, and incubated for 2 hr under gentle

190   agitation at RT in the secondary antibody solution containing 2% (v/v) normal horse serum,

191   0.4% (v/v) Triton X-100, and the secondary antibodies. For the biocytin-filled cells the

9

192   streptavidin conjugate was also added at this step. The slices were washed once for 10 min at

193   RT with PBS, and incubated for 10 min RT in 0.3 µM DAPI (D3571, Invitrogen) in 0.1 M PB.

194   Sections were then washed three times at RT with 0.1 M PB, mounted on glass coverslips with

195   gelatin-chrome alum, air-dried, and closed with Mowiol mounting solution containing 10%

196   (w/v) Mowiol 4-88, 25% (v/v) glycerol in 0.1 M Tris-buffer (pH 8.5). Sections were kept at 4 °C

197   in the dark until further use.

198   ***Confocal and structured illumination imaging***

199   Confocal imaging was done on a Zeiss LSM 700 microscope equipped with a plan-apochromat

200   20x, 0.75 NA and a 63x, 1.4 NA objective, and PMT detectors, or on a Zeiss Elyra PS1

201   microscope, which is described below. Confocal images were acquired with optimized settings

202   for laser power, detector gains and pin hole diameters. Large (2048x2048 pixels), high-

203   resolution images were acquired with a pixel size of 0.041 µm laterally and 0.110 µm radially

204   to facilitate the comparison with structured-illumination microscopy (SIM) images. Low-

205   resolution tile images were acquired with a pixel size of 0.274 µm.

206   Structured-illumination imaging was done on a Zeiss Elyra PS1 system equipped with 488, 561

207   and 642 nm, 100 mW diode lasers; fluorescence was acquired with a Zeiss plan-apochromat

208   63x, 1.4 NA objective and an Andor iXon DU 885 EMCCD camera (1002 x 1004 pixels). Gratings

209   were presented at 5 phases and 5 rotations for every depth. Sampling interval was 110 nm

210   axially and the reconstructed super-resolution image has a pixel size of 41 nm. The fluorophore

211   signals were acquired sequentially. Reconstructions were made with built-in algorithms using

212   ZEN 2012 SP1 black (v8.1.3.484).

213   ***Electrophysiological analysis***

214   EPSPs were detected as described previously (Sierksma *et al.*, 2016) using an EPSP minimal

215   rate of rise (>0.7 V/s) and an EPSP onset based on the third derivative. EPSPs that were present

216   between 1 to 8 ms post-stimulation were categorized as 'evoked' EPSPs. We grouped the

217   evoked EPSPs based on stimulus strength, latency and rate of rise. We assumed that with

218   increasing stimulation intensities previously-recruited inputs would still be activated. For

219   consecutive stimulus intensities Welch's *t* was calculated for the EPSP latency and the rate of

220   rise, and both *t* values were added together. When the summed *t* value was above 6 and the

221   increase of the response rate of rise was >20%, we considered the evoked EPSPs to differ from

222   each other. We visually checked whether this difference was due to a new input or just a shift

223   in activation probability of a previously activated input. For a new input its EPSP rate of rise

224   was calculated by subtracting the EPSP rates of rise of previously identified inputs when they

225   were of similar latencies (±0.5 ms). For four recordings we found EPSPs with longer latencies

226   (Figure 1C), and for these recordings the Welch's *t* test was calculated but restricted to a

227   latency domain defined by the experimenter. For the example in Figure 1C this was 1-3 ms.

228   Lastly, the EPSP rate of rise of an input was checked against the distribution of spontaneously-

229   occurring EPSP rates of rise, and the defined input was only accepted if spontaneous EPSPs

230   with similar rates of rise were recorded.

231   In addition to the inputs identified by stimulation, we identified inputs from the spontaneous

232   EPSPs. By comparing the distribution of EPSP rates of rise of all detected EPSPs in a recording

233   with the evoked EPSPs, we could sometimes identify additional strong inputs (8 strong inputs

234   in 8 cells). Within the spontaneous EPSPs, many had a small size (0.7-2 V/s), and these inputs

235   were therefore hard to distinguish individually. If small EPSPs were not evoked, we visually

236   selected peaks from the distribution of the EPSP rate of rise (Figure 1C-D) to define these

237   smaller inputs, and added them to the dataset to acknowledge their existence. However, the

238   inputs with small EPSPs were hard to demarcate and therefore likely underestimated.

239   Based on the EPSP size analysis, we identified on average 5.6 inputs per cell. For comparison,

240   prior to synaptic elimination 5-12 axons contact a principal neuron in EM studies of the mouse

241   MNTB (Hoffpauir *et al.*, 2006). Another measure for how well we can identify all inputs can be

11

242   obtained by comparing spontaneous and evoked inputs. In 8 out of 22 cells we were unable to

243   activate the strongest input that was observed among the spontaneous activity, indicating that

244   on the order of one in three inputs (8 out of 22 strongest inputs) were not electrically

245   stimulated. Spontaneous activity partially negated this problem, but may have introduced a

246   bias towards the most active and stronger inputs (see also below). To what extent synaptic

247   inputs of the principal neuron are active in every spontaneous activity burst is unknown, but

248   anecdotal evidence showed extensive co-occurrence of two distinct, large inputs during

249   spontaneous bursts (Sierksma *et al.*, 2016).

250   We tested whether the strong inputs could be further subdivided based on the presence of

251   inter-event intervals that were shorter than the refractory period or the silent period within

252   minibursts (Sierksma *et al.*, 2016), but this did not lead to the identification of additional

253   connections. Altogether, we believe that our combined analysis of spontaneous and evoked

254   responses identified most synaptic inputs, except for some smaller inputs.

255   ***Image analysis***

256   Analysis of 3D-SIM image stacks was done in ImageJ using the FIJI framework (Schindelin *et al.*,

257   2012; Schneider *et al.*, 2012), making use of two custom-made 3D segmentation ImageJ

258   plugins (available at: https://github.com/ErasmusOIC/FloodFill3D,

259   https://github.com/ErasmusOIC/Sphere_Floodfill). In brief, we first segmented the cell body

260   using the biocytin signal with the Sphere_Floodfill plugin. The biocytin signal was scanned with

261   a 400 nm (10 pixels)-radius sphere. If 40% of the sphere contained intensity values above

262   threshold, its center was assigned to the cell body. To segment the VGluT signal in 3D, we used

263   the FloodFill3D plugin which scans all 26 neighboring pixels and assigns them to the VGluT

264   structure if they are above an intensity threshold determined using the IsoData-method of

265   ImageJ. To account for the width of the synaptic cleft, the cell body was enlarged by dilation.

266   The amount of dilation (range 160-760 nm) was determined for each cell by maximizing the

267   fraction of the dilated cell body covered by the VGluT structures. Where needed, axonal

268   biocytin signals were manually removed from the cell body. The fraction of the surface area of

269   the cell body that was covered by the VGluT clusters was calculated.

270   All images were pseudo-colored and contrasted in ImageJ. Color gamma enhancement was

271   performed with Adobe Photoshop 19.1.0. We noticed that the peak intensities of Piccolo and

272   VGluT did not seem to overlap in SIM images. From line profiles it became clear that Piccolo

273   labeling did overlap with VGluT at lower intensities, but not at the highest VGluT intensities.

274   **Statistics**

275   No blinding was applied to the analysis. Linear regression analyses against pup age were

276   performed for the developmental effects. When the developmental effect was significant, the

277   slope of the fit is reported; when not, the average is reported, and subsequently the F-statistic

278   with the degrees of freedom, and the p-value are reported. Subsequent testing on the same

279   data was Bonferroni-corrected, and are reported as 'corrected p'. Correlations are reported as

280   Pearson's r or Spearman's ρ after rank transformation. To compare prespike-associated strong

281   inputs with the other strong inputs, we performed Welch's t-test for the EPSP amplitude and

282   latency. EPSP rate of rise and synaptic efficacy to trigger postsynaptic firing (P_{AP}) were

283   correlated with age. Age correction was performed by adding age as an explanatory variable to

284   the regression analysis. P_{AP} was judged to have non-normally distributed residuals and

285   therefore the regression analysis was done on the ranks. The F-statistic of the regression and

286   the effect of prespike variable within this regression are reported. Sigmoid and linear fits were

287   performed with Igor Pro 6.37 (WaveMetrics Inc.). To correlate the competition index with

288   relative coverage we used Spearman's ρ. p-values < 0.05 were considered significant.

13

289   **Results**

290   ***Postsynaptic responses of* in vivo *stimulated fibers***

291   We made *in vivo* whole-cell recordings from principal neurons in the rat MNTB around the

292   time the calyx of Held synapse forms. A bipolar stimulation electrode was placed

293   contralaterally from the recording site to distinguish inputs based on their threshold for axonal

294   action potential generation (see Methods; Figure 1A). Above a threshold of 83 ± 19 μA (mean ±

295   SD, *n* = 30 animals, range: 65-140 μA) a field potential could be evoked in the MNTB. In a total

296   of 22 MNTB cells, EPSPs could be evoked, and with increasing current stimulation we typically

297   observed either the presence of a large, all-or-none, calyceal-like input, or more graded

298   increases in EPSP size (Figure 1B). In both cases the evoked responses often could reach AP

299   threshold (*n* = 16 of 22 cells). To identify the different inputs, we looked for discontinuities in

300   the rates of rise and/or the latency of the evoked responses following an increase in stimulus

301   intensity, as detailed in the Methods; these discontinuities were interpreted as the

302   recruitment of a new input. A comparison of the rates of rise of the evoked EPSPs with those

303   of the spontaneously-occurring EPSPs was used as a further check on the accuracy of the

304   identified inputs (Figure 1C-D). In 8 out of the 22 cells we were unable to observe the largest

305   spontaneous EPSPs following the electrical stimulation, suggesting that we failed to activate

306   the strongest input for these cells. EPSP subpopulations were found with typical latencies of 1-

307   3 and 4-8 ms (Figure 1E), as described in slice studies (Banks & Smith, 1992; Hoffpauir *et al.*,

308   2006; Marrs & Spirou, 2012). The large EPSPs always belonged to the subpopulation with 1-3

309   ms delays (Figure 1E). On average the EPSP latencies became smaller during the first postnatal

310   week (Figure 1F). In addition to early myelination (Rozeik & Von Keyserlingk, 1987; Hamano *et*

311   *al.*, 1996), an increase in axon diameter and/or ion channel densities may have contributed to

312   this decrease in latency. The different subpopulations may reflect different developmental

313   stages among the calycigenic axons.

14

314   Within this developmental period the principal neuron passes through a stage of exuberant

315   synaptic connectivity (Holcomb *et al.*, 2013). In addition to the 22 cells in which we recorded

316   both evoked and spontaneous EPSPs, we recorded in 10 cells only the spontaneous activity. In

317   total, we identified 180 putative inputs in 32 cells, 5.6 ± 1.6 per cell (mean ± SD). The

318   distribution of input rate of rise was skewed to the right (Figure 2A). By sorting all inputs on

319   their mean rate of rise, a discontinuity was observed at about 10 V/s (Figure 2A-B), which we

320   used as a threshold to distinguish between weak and strong EPSPs. To have a measure of

321   synaptic competition, we calculated the competition index, defined as the ratio of the rates of

322   rise of the second strongest and the strongest input (Figure 2C). The competition index ranges

323   from 1 to 0, where 1 indicates an equal rate of rise of the two strongest inputs, while if the

324   competition index approaches 0 the strongest input has outcompeted the second strongest

325   input in strength. The competition index decreased during development (-0.07 ± 0.02 day^{-1}, n =

326   32 cells, $F_{1,30}$ = 11, p = 0.002). This decrease can signify both an increase of the rate of rise of

327   the strongest input and a reduction for the second strongest input. We therefore plotted the

328   two against each other (Figure 2D). The rate of rise of the strongest input clearly increased

329   during development (4.2 ± 1.1 V s^{-1} day^{-1}, $F_{1,30}$ = 14, corrected p = 0.001), while the rate of rise

330   of the second strongest did not change (3.7 ± 0.2 V/s, $F_{1,30}$ = 2.1, corrected p = 0.3). This was

331   not related to a difference between evoked and spontaneous inputs, because inputs, whether

332   evoked or identified within spontaneous activity, had similar rates of rise for both the

333   strongest (stim.: 19 ± 10 V/s, n = 14 cells; spont.: 16 ± 12 V/s, n = 18 cells) and the second

334   strongest input (stim.: 3.6 ± 1.2 V/s, n = 14; spont.: 3.7 ± 1.2 V/s, n = 18). In contrast to what

335   may have been expected for competing inputs, the developmental increase in strength of the

336   strongest input did not coincide with a decrease in the second strongest input.

337   ***Strong inputs and prespikes***

338   The effects of electrical stimulation of the calyx of Held synapse have been extensively studied

339   in slices (Borst & Soria van Hoeve, 2012), but equivalent *in vivo* recordings have not yet been

15

340 reported. In nine cells we could activate an input associated with an EPSP >10 V/s that could

341 easily be distinguished from the other EPSPs. These inputs could be activated with a threshold

342 current of 0.24 ± 0.09 mA (mean ± SD; n = 9 inputs in 9 cells, range 0.12 – 0.40 mA), although

343 the reliability of activation with current above threshold varied between pups (83 ± 12% of the

344 stimulations, mean ± SEM; range 59-100%). The average latency of the input's EPSP was 2.1 ±

345 0.3 ms (mean ± SD, n = 9 inputs in 9 cells, range 1.6 – 2.5 ms) with little jitter between trials

346 (SD/mean: 2.3 ± 0.9%, n = 9 inputs, range 1.0-3.8%). Given the distance of 500-1000 µm

347 between the stimulation and recording electrode and a synaptic delay of ~0.5 ms, the

348 propagation speed can be estimated to be in the order of 1 m/s. The AP travel time became

349 less variable with development (n= 9 inputs in 9 cells, jitter vs. age, r = -0.75, -0.7 ± 0.2% per

350 day, $F_{1,7}$ = 9.0, p = 0.02). In addition, a decrease in latency (r = -0.7, -0.18 ± 0.07 ms/day, $F_{1,7}$ =

351 5.6, p = 0.05) suggested a developmental increase in conduction speed. This increase is likely

352 underestimated, as we positioned the stimulation electrode as contralaterally as was

353 permitted by the cranial window to be able to separate the stimulus artefact from the

354 responses. These developmental changes will contribute towards the precise timing of the

355 calyx of Held in adult, hearing animals.

356 The calyx of Held can typically be identified in postsynaptic recordings by the presence of a

357 prespike, a small deflection preceding the large EPSPs (Forsythe, 1994; Borst *et al.*, 1995;

358 Lorteije *et al.*, 2009). Prespikes can already be detected in the first postnatal week (Crins *et al.*,

359 2011; Sierksma *et al.*, 2016). We therefore inspected every strong input whether a prespike

360 was present (Figure 3A). In four of four cells >P5, six of ten cells of P4-5, and in none of six P2-3

361 cells large EPSPs were preceded by a prespike (Figure 3B). Hence, the presence of the prespike

362 before a large EPSP was more likely at older ages (r = 0.6); a fit with a logistic function yielded a

363 mid-point of 4.1 ± 0.4 days postnatally (mean ± SD) and a steepness of 0.7 ± 0.4 days,

364 suggesting that within two days most strong inputs will become associated with a prespike.

365 The prespike can be considered to be a sensitive indicator of the currents that flow across the

16

366   release face. As a consequence, this developmental switch may be explained by an increase in

367   these currents. The size of these currents depends on apposition area (Hoffpauir *et al.*, 2006;

368   Holcomb *et al.*, 2013), time course of the calyceal AP, which accelerates considerably during

369   early development (Taschenberger & von Gersdorff, 2000; Sierksma & Borst, 2017),

370   isochronicity of the presynaptic currents, and the subcellular distribution of presynaptic ion

371   channels. In addition, the coupling depends on synaptic cleft resistivity and postsynaptic

372   admittance (Savtchenko, 2007). The rapid change in most of these properties during this

373   period should underlie the emergence of the prespike.

374   As we observed strong inputs with and without prespike, we asked whether their properties

375   were different. For the inputs that were electrically stimulated, the strong inputs with and

376   without a prespike had a latency of 2.1 ± 0.4 ms and 2.2 ± 0.3 ms, respectively (Figure 3C, n = 4

377   and 5 inputs in 4 and 5 cells, respectively; t_7 = 0.5, r = -0.2, p = 0.7). For the EPSP rate of rise,

378   amplitude and the efficacy to trigger a postsynaptic AP (P_{AP}), we included the strong inputs

379   that were identified in the spontaneous activity. The EPSP rate of rise was 28 ± 2 V/s versus 19

380   ± 2 V/s (Figure 3D, age correction, n = 20 inputs in 20 cells, $F_{2,17}$ = 5.3, effect of prespike, 5 ± 4

381   V/s, t_{17} = 1.2, p = 0.3) and had a coefficient of variation in the range of 7-38%. EPSP amplitude,

382   which did not significantly correlate with age (r = 0.2), was 19.6 ± 1.1 mV versus 15.6 ± 1.5 mV

383   (n = 10 and 10 inputs in 10 and 10 cells; t_{18} = 2.1, r = 0.45, p = 0.06). As these EPSPs typically

384   triggered an AP (75 ± 31%, mean ± SD; range 11-100%), their amplitudes are underestimated.

385   The fraction of EPSPs that triggered a postsynaptic AP was 0.88 ± 0.22 versus 0.63 ± 0.34

386   (Figure 3E, n = 20 inputs in 20 cells, rank-transform and age correction, $F_{2,17}$ = 5.4, effect of

387   prespike: 7 ± 3, t_{17} = 2.6, p = 0.02). Overall, prespike-associated inputs triggered postsynaptic

388   activity more effectively. Still, some inputs that did not generate a detectable prespike were

389   comparable to the calyceal inputs in strength and efficacy, as we observed before (Sierksma *et*

390   *al.*, 2016). Do these strong inputs without prespikes correspond to calyx of Held synapses? To

391   answer this question, we looked at the synaptic structure of the recorded cells.

392 **_The active zone protein Piccolo in the neonatal auditory brainstem_**

393 The dramatic developmental change in the glutamatergic innervation of MNTB neurons can be

394 visualized by VGluT immunolabeling (Rodríguez-Contreras *et al.*, 2008). However, VGluT does

395 not mark release sites or postsynaptic densities. Wherease some postsynaptic density proteins

396 appear delayed compared to VGluT labeling (Soria Van Hoeve & Borst, 2010), Piccolo, an active

397 zone protein, was recently shown to be already present in P9 calyces (Dondzillo *et al.*, 2010).

398 We tested whether Piccolo could be used to visualize the release face of terminals within the

399 first neonatal week. Already at P3-4, Piccolo-labeling was found throughout the superior

400 olivary complex (SOC) in most auditory nuclei (*n* = 8 rats; Figure 4A). Although the staining was

401 not particularly strong in the MNTB, it clearly co-labeled large perisomatic structures

402 containing VGluT (Figure 4B). As early as P2, the Piccolo labeling could delineate an edge of the

403 larger VGluT-clusters (Figure 4C, *n* = 2 of 5 P2 animals). Piccolo puncta were also found outside

404 the somatic regions of the MNTB, and a Piccolo punctum was occasionally found within the

405 soma of a principal cell (Figure 4C). Generally, when imaged with confocal microscopy, the

406 Piccolo edges appeared to be composed of individual spots, which were close to the diffraction

407 limit (Figure 4C-D). We turned to structured-illumination microscopy (Gustafsson, 2005), which

408 revealed that the Piccolo clusters were indeed composed of multiple spots (Figure 4D). These

409 spots were also found in biocytin-filled calyces, indicating that Piccolo can be present in the

410 active zones of the calyx of Held at P5 (*n* = 11 of 12 calyces; Figure 4E). Piccolo thus identifies

411 the release face of synapses and thereby facilitates the identification of the target neuron in

412 the case of axosomatic VGluT clusters (Figure 4C-D). However, dendritic synapses could not be

413 reliably identified without labeling the postsynaptic neuron.

414 **_Structure-function correlation within and across cells_**

415 From the 32 recorded cells, we recovered 20 cells with immunolabeling for VGluT (1 P2, 7 P3, 8

416 P4, 2 P5, 1 P6, 1 P7). For these cells we segmented the soma and the VGluT clusters

417 surrounding the soma using a new, semi-automatic procedure (see Methods, Figure 5A). This

18

418   segmentation takes into account that a VGluT cluster may have multiple contact points with

419   the soma by clustering connected voxels. A VGluT cluster is thus defined as a contiguous

420   structure of VGluT-positive voxels and VGluT clusters, by definition, were not in contact with

421   each other. The total somatic surface was 620 ± 230 μm^2 (mean ± SD, n = 20), which is

422   comparable to earlier estimates (Sommer *et al.*, 1993; Hoffpauir *et al.*, 2006). We observed

423   that multiple VGluT clusters contacted the postsynaptic cell, of which most had a postsynaptic

424   contact area <3 μm^2 (Figure 5B-C). The total postsynaptic area that was covered by VGluT

425   ranged from 2.4 μm^2 to 76.5 μm^2. As calyces can cover >50% of the soma (Sätzler *et al.*, 2002;

426   Hoffpauir *et al.*, 2006), our segmentation of VGluT thus may give us only a lower-bound

427   approximation of its size. For each cell we identified the largest and second largest VGluT

428   cluster. The contact area of the largest cluster on the postsynaptic cell ranged from 0.4 μm^2 to

429   59.7 μm^2 (13 ± 16 μm^2, mean ± SD). For the second largest cluster it ranged from 0.3 μm^2 to

430   10.0 μm^2 (2.4 ± 2.8 μm^2, mean ± SD). For 3 cells the Piccolo labeling failed. For 9 cells we could

431   see clear Piccolo labeling coinciding with the largest VGluT cluster directed towards the

432   biocytin-filled cell. For 8 cells VGluT clusters surrounding the biocytin-labeled soma did not

433   show clear Piccolo labeling, but Piccolo coincided with VGluT in the surrounding tissue. The

434   signal-to-noise ratio of the reconstruction did not allow a more in-depth analysis of the Piccolo

435   clusters.

436   If the size of the VGluT cluster is a useful estimate of the size of the terminal, then it should

437   predict the presence and amplitude of a prespike in our *in vivo* recordings. The size of the

438   VGluT cluster was moderately correlated with the presence of a prespike (ρ = 0.63). The largest

439   VGluT cluster was 28 ± 19 μm^2 (mean ± SD) for the 5 cells in which we recorded a prespike.

440   This was significantly larger than in the 15 cells without a prespike (8 ± 11 μm^2, mean ± SD, t_{18}

441   = 3.3, *p* = 0.004). Next, we compared the prespike peak-to-peak amplitude with the size of the

442   largest VGluT cluster. We excluded one of the recordings, in which the prespikes had an

443   amplitude of 15 mV. In this recording a small patch of calyceal membrane may have been

19

444   present within the electrode tip (Forsythe, 1994). As the calyx was not stained for biocytin, the

445   membrane of the calyx was apparently not damaged by the pipette. For the remaining

446   prespikes the average amplitudes were 0.11, 0.26, 0.30 and 0.37 mV, which corresponded with

447   values of 19.2, 23.1, 25.6 and 59.7 μm^2 for the largest VGluT cluster ($r = 0.8$). Because of the

448   small number of observations, this correlation did not reach significance ($F_{1,2} = 3$, $p = 0.2$). Also,

449   we observed VGluT clusters with similar contact area among the cells from which we did not

450   record a prespike. Altogether, the size of the largest VGluT cluster may indicate the presence

451   of a large terminal, but it is unlikely to reveal the entire contact area made by the terminal.

452   As synaptic strength depends more on glutamate release than on terminal size, the observed

453   VGluT cluster may still be a good approximation of synaptic strength. We therefore compared

454   synaptic strength with the contact area of VGluT clusters (Figure 5D). The size of the strongest

455   input was correlated to the size of the largest VGluT cluster (log-transform, $r = 0.8$, $F_{1,18} = 26$, p

456   < 0.001). The structure-strength relation could be approximated by EPSP (V/s) $= \beta$ area$^\alpha$ with β

457    $= 6.8 \pm 0.9$ V s^{-1} $\mu m^{-2\alpha}$ and $\alpha = 0.35 \pm 0.06$. Thus, the input strength was correlated with the

458   cube root of VGluT area. For the older pups (2 P5, 1 P6 and 1 P7 cell) the structure-function

459   relation was underestimated; three of four synapses were stronger than expected from their

460   apposition area. This may indicate that there is a developmental change in the structure-

461   function relation or that the total vesicle-loaded contact of giant synapses is underestimated

462   as the largest VGluT cluster may be only a small part of the synapse.

463   Calyces that innervate a multi-calyceal principal cell are filled with synaptic vesicles (Holcomb

464   *et al.*, 2013), and would thus be expected to be observed with VGluT labeling. The different

465   calyces were observed to each occupy a contiguous area, sometimes at opposite sides of the

466   target neuron (Holcomb *et al.*, 2013). This type of multi-calyceal innervation was not observed

467   here (Figure 5B, C and E). As we cannot be sure whether individual VGluT clusters are

468   independent inputs or belong to the same synapse, we cannot use the second largest VGluT

20

469   clusters to relate to the physiology. Indeed, the size of the second largest VGluT cluster was

470   not correlated with the size of the second strongest input (r = -0.1, $F_{1,16}$ = 0.3, p = 0.6).

471   Nonetheless, for multi-calyceal innervation we would have expected to observe two large

472   VGluT clusters of comparable contact area (Figure 5E). No pair of VGluT clusters was

473   unambiguously identified as such.

474   As we cannot conclusively assign a VGluT cluster to individual inputs, it may still be that the

475   second calyx contacted the cell via multiple clusters. We therefore quantified how the largest

476   VGluT cluster relates to all the other clusters that contact the soma of the same target neuron

477   as the contact ratio of the contact area of the largest VGluT cluster to the total somatic surface

478   contacted by VGluT. When the contact ratio approaches 100% the largest VGluT cluster is the

479   only cluster that contacts the soma of the target neuron, and values <100% indicate the

480   presence of additional VGluT clusters which may or may not belong to the same terminal. The

481   contact ratio ranged from 9-98% (41 ± 30%, mean ± SD) and was negatively correlated to the

482   competition index (Figure 5F, $F_{2,17}$ = 10, p = 0.0012, age correction, ρ = -0.7). With these two

483   measures, the competition index and the contact ratio, we could have identified multi-calyceal

484   competition as (*i*) two terminals that cover about an equal size of the soma, *i.e.* a contact ratio

485   of ~0.5, and (*ii*) two inputs of similar strength, giving a competition index close to 1 (shaded

486   area in Figure 5F). Such combinations were not observed. We thus conclude that we did not

487   find strong evidence in support of multi-calyceal competition. In addition, there were no large

488   discrepancies between the structure and function of the developing calyx of Held synapse. This

489   suggests that in the developing rat MNTB a large VGluT cluster likely indicates the presence of

490   a strong input that is clearly stronger than the other inputs of its target neuron.

Discussion

491

492 In this study we combined *in vivo* electrophysiology with immunolabeling of the developing

493 calyx of Held synapse. With afferent stimulation we identified multiple inputs for each

494 principal neuron. Increasing stimulation levels showed either a graded increase or a sudden,

495 large jump in the rate of rise of the response. The strongest inputs across cells showed a

496 shorter latency. The strongest inputs were typically at least twice as strong as the other inputs.

497 This divergence increased during development with little change in the strength of the second

498 strongest input. We found that in the first postnatal week Piccolo is already present within

499 perisomatic VGluT clusters, which are putative calyceal terminals. The contact surface of the

500 largest VGluT cluster correlated with the strength of the strongest input *in vivo*. Furthermore,

501 the relative coverage of the largest VGluT cluster correlated with the relative strength of the

502 strongest to the second strongest input. Overall, VGluT-positive structures correlated with

503 synaptic strength *in vivo*. The association of a strong input with a prespike became more likely

504 during development. Prespike-associated inputs were more effective in triggering postsynaptic

505 activity, but some inputs without a prespike had similar properties.

506 ***Calyceal competition during development?***

507 The prevalence of multiple calyces on a principal MNTB neuron is a subject of debate. On the

508 one hand, multiple strong inputs have been observed in slice recordings (Bergsman *et al.*,

509 2004; Hoffpauir *et al.*, 2006; Hoffpauir *et al.*, 2010), and structural evidence for the presence of

510 multiple large terminals on rodent MNTB neurons has also been obtained (Wimmer *et al.*,

511 2004; Hoffpauir *et al.*, 2006; Holcomb *et al.*, 2013; Matho, 2013; Milinkeviciute *et al.*, 2019).

512 Although only a minority (up to 10%) of neurons is persistently innervated by multiple calyces

513 (Holcomb *et al.*, 2013; Matho, 2013; Milinkeviciute *et al.*, 2019), as many as half of the

514 principal neurons are putatively contacted by multiple large terminals during development

515 (Holcomb *et al.*, 2013). On the other hand, to our knowledge not a single conclusive example

516 of multi-calyceal innervation has been reported for *in vivo* studies of the adult MNTB. Multi-

22

517   calyceal innervation could have been observed as inputs associated with prespikes that do not

518   obey the (relative) refractory period. Neither our *in vivo* recordings nor our VGluT labeling

519   revealed multi-calyceal innervation in this study. Multi-calyceal competition would be

520   expected to involve an input strength that is within a similar range. This was observed in our

521   earlier study where three out of 132 cells had two strong inputs that could be separated based

522   on the presence or absence of a prespike and that defied the refractory period (Sierksma *et al.*,

523   2016). However, we cannot exclude that one of these inputs was dendritic. Even if we grant

524   that these three cells demonstrate multi-calyceal competition, we identify, from our earlier

525   (3/132 cells) and the current (0/32 cells) experiments, <10% of rat principal neurons with

526   multi-calyceal innervation during development. These values are comparable to the 1%

527   reported in a pre-hearing mouse study (Kronander *et al.*, 2019) and to our earlier study in P9

528   rats, in which 1 of 86 cells showed two large, perisomatic VGluT clusters for (Rodríguez-

529   Contreras *et al.*, 2006). Even though we cannot exclude having missed calyces due to low

530   VGluT expression, we conclude that multi-calyceal competition is unlikely to significantly

531   contribute to the development of the rat calyx of Held synapse.

532   The presence of competition has been evaluated by the (relative) contact surface (Holcomb *et*

533   *al.*, 2013) or by the (relative) strength of the inputs (Hoffpauir *et al.*, 2010; Sierksma *et al.*,

534   2016). Here, we compared a structural and a functional measure for competition, and

535   generally observed a good match between the two. Although immunolabeling did not allow

536   the unambiguous identification of different inputs based on the VGluT clusters, we did observe

537   a clear match between VGluT relative coverage and the competition index, indicating a link

538   between the physiological and morphological development of the MNTB synapses. In addition,

539   it may point to a possible period of competition prior to calyx formation as we only observed

540   inputs with competing strength at P2-3, when the relative coverage of the largest VGluT

541   cluster was still low and only few calyces have already formed (Morest, 1968; Kandler & Friauf,

542   1993; Rodríguez-Contreras *et al.*, 2008).

23

543   For two other giant, mono-innervating synapses, the neuromuscular junction (NMJ) and the

544   cerebellar climbing fiber-Purkinje cell synapse (CF-PC), different types of competition have

545   been described. In the case of NMJ, before mono-innervation is established, one input

546   becomes >4 fold stronger than the other ones by both an increase of the strongest and a

547   decrease in the strength of the other inputs (Colman *et al.*, 1997). As NMJ inputs compete for a

548   small patch of the muscle membrane (Sanes & Lichtman, 1999; Darabid *et al.*, 2014), the

549   expansion of one NMJ necessarily involves the shrinkage of another, as reflected in the

550   opposing changes in strength. In contrast, CFs compete at the soma for access to the apical

551   dendrite (Watanabe & Kano, 2011). A fourfold strengthening of the strongest input was

552   observed during development (Hashimoto & Kano, 2003) while other inputs remained

553   constant (Bosman *et al.*, 2008). Subsequently, one of the immature CFs is allowed to

554   translocate to the apical dendrite (Hashimoto *et al.*, 2009; Watanabe & Kano, 2011), ending

555   the competition (Carrillo *et al.*, 2013). Our observations seem to reflect a CF-PC-like

556   competition. We observed that the strongest input became >4 times stronger than the other

557   inputs between P3-5 without a substantial change for the second strongest. This may indicate

558   that they do not compete for overlapping synaptic domains (Holcomb *et al.*, 2013). In addition,

559   the strongest input already reached this relative strength while its coverage still seemed to be

560   low, suggesting that the increase in strength precedes and instructs the expansion (Hoffpauir

561   *et al.*, 2010). In contrast, the combination of a large VGluT cluster with a high competition

562   index was not observed, suggesting that somatic expansion and/or VGluT filling of the terminal

563   (Rodríguez-Contreras *et al.*, 2008) represents a relatively late maturation stage.

564   An important role for exuberant connectivity seems to be to provide sufficient candidate

565   precursors to ensure that each principal neuron will eventually end up being innervated by a

566   calyx of Held from a globular bushy cell that innervates only a limited number of other

567   principal neurons. As the molecular mechanisms underlying this process are gradually being

568   elucidated (Hsieh *et al.*, 2010; Nakamura & Cramer, 2011; Ehmann *et al.*, 2013; Michalski *et al.*,

569   2013; Xiao *et al.*, 2013; Körber *et al.*, 2014; Yu & Goodrich, 2014; Nothwang *et al.*, 2015;

570   Willaredt *et al.*, 2015; Dimitrov *et al.*, 2016), to what extent postsynaptic activity plays a role in

571   this selection process is still unclear. Without concurrent activity of other inputs, non-calyceal

572   inputs are unable to evoke postsynaptic APs, as they elicit postsynaptic firing almost

573   exclusively by EPSP summation (Sierksma *et al.*, 2016 and this study). In the fruit fly

574   postsynaptic activity stimulates the release of bone morphogenetic protein (BMP) homologue

575   which promotes active zone development and NMJ growth (Berke *et al.*, 2013; Berke *et al.*,

576   2020). Mice conditionally deleted for BMP receptor 1 and 2 show deficits in transmitter

577   release and smaller calyces (Xiao *et al.*, 2013) in addition to a persistence of axonal branches

578   with calyces and increased multi-calyceal innervation (Kronander *et al.*, 2019). Similarly,

579   calyces fail to form when synaptic transmission is impaired by genetic deletion of dynamins

580   (Fan *et al.*, 2016). These phenotypes may reflect a need for postsynaptic activity in calyx

581   development.

582   Following calyx formation, most non-calyceal inputs are gradually pruned over a prolonged

583   period (Morest, 1968; Kandler & Friauf, 1993; Rodríguez-Contreras *et al.*, 2008), whereas some

584   may persist (Guinan & Li, 1990; Hamann *et al.*, 2003). This pruning phase may be mediated by

585   microglia (Milinkeviciute *et al.*, 2019).

586   ***Structure-function relation for the developing calyx of Held synapse***

587   The presence of a prespike indicates the innervation by a giant terminal (Forsythe, 1994). In

588   this study four cells with a prespike-associated input had a large VGluT cluster and one cell did

589   not. Possibly in the latter case the terminal was larger than revealed by VGluT labeling

590   (Rodríguez-Contreras *et al.*, 2008). Conversely, four cells were observed where the presence of

591   a large VGluT cluster did not match with a prespike-associated input. In these cases we may

592   have missed small prespikes due to the capacitive filtering by the soma, and the prespikes may

593   have been detectable in voltage-clamp recordings. There are also a number of other biological

594   factors that influence the prespike amplitude (see Results), but experimental observations on

595   the relation between presynaptic AP and the prespike have so far been qualitative (Forsythe,

596   1994; Borst *et al.*, 1995; Wang *et al.*, 2017). Whereas the presence of a clear prespike seems to

597   be good evidence for the presence of a giant somatic terminal, experimental and

598   computational studies on the prespike (Savtchenko, 2007) based on exact morphology (Spirou

599   *et al.*, 2008) are needed to allow a more precise estimate for the minimal conditions under

600   which a calyx generates a prespike.

601   From our structure-function analyses we found that VGluT labeling closely follows the strength

602   of the strongest input. This VGluT cluster represents the total pool of glutamatergic vesicles in

603   the calyx of Held (Rodríguez-Contreras *et al.*, 2008). This pool likely covers multiple active

604   zones (Sätzler *et al.*, 2002; Taschenberger *et al.*, 2002; Hoffpauir *et al.*, 2006; Dondzillo *et al.*,

605   2010), which we observed with the Piccolo labeling. The relation between the size of this pool

606   and synaptic strength is complex, depending on among others quantal size, release probability,

607   and number of release sites (Atwood & Karunanithi, 2002; Schneggenburger & Forsythe, 2006;

608   Borst & Soria van Hoeve, 2012). We found a cube root relation between VGluT contact surface

609   and EPSP rate of rise, suggesting that the increase in vesicle pool is relatively ineffective in

610   increasing synaptic strength. An important factor may have been that EPSC-EPSP relation

611   saturates for large EPSCs (Lorteije *et al.*, 2009; Sierksma *et al.*, 2016), which would lead to a

612   sublinear relation between quantal content and EPSP size. During early development quantal

613   size is stable (Chuhma & Ohmori, 1998; Taschenberger & von Gersdorff, 2000) or may slightly

614   decrease (Rusu & Borst, 2011), while the active zones and postsynaptic densities become more

615   numerous and segregate into smaller clusters (Taschenberger *et al.*, 2002; Hoffpauir *et al.*,

616   2006; Soria Van Hoeve & Borst, 2010). Other possible factors include changes in release

617   probability, homeostatic plasticity of postsynaptic excitability (Hoffpauir *et al.*, 2010; Rusu &

618   Borst, 2011; Sierksma *et al.*, 2016) or a contribution of dendritic inputs (Rodríguez-Contreras *et*

619   *al.*, 2008; Holcomb *et al.*, 2013).

26

620   For the study of the relationship between structure and function, the calyx of Held synapse has

621   the advantage of an axosomatic, (putative) one-to-one innervation facilitating the

622   identification of the strongest input *in vivo* with the largest cluster *ex vivo*. An even more direct

623   relationship might be possible following simultaneous electrophysiology and calcium imaging

624   *in vivo* (Winnubst *et al.*, 2015). Subsequent reconstruction of the synapses after *in vivo* imaging

625   (Liang *et al.*, 2018) would allow a structure-function description for multiple synapses of a

626   single cell. Such studies may further define the relationship between morphological and

627   functional properties of the precursors of the calyx of Held. Finally, longitudinal imaging might

628   reveal some of the dynamics associated with the formation of the calyx of Held and the

629   interactions with surrounding axons (Rodríguez-Contreras *et al.*, 2008).

27

630 **References**

631 Atwood HL & Karunanithi S. (2002). Diversification of synaptic strength: presynaptic elements.
632   *Nat Rev Neurosci* **3,** 497-516.

633 Banks MI & Smith PH. (1992). Intracellular recordings from neurobiotin-labeled cells in brain
634   slices of the rat medial nucleus of the trapezoid body. *Journal of Neuroscience* **12,**
635   2819-2837.

636 Bergsman JB, De Camilli P & McCormick DA. (2004). Multiple large inputs to principal cells in
637   the mouse medial nucleus of the trapezoid body. *J Neurophysiol* **92,** 545-552.

638 Berke B, Le L & Keshishian H. (2020). Target-dependent retrograde signaling mediates synaptic
639   plasticity at the *Drosophila* neuromuscular junction. *Developmental Neurobiology***,** in
640   the press.

641 Berke B, Wittnam J, McNeill E, Van Vactor DL & Keshishian H. (2013). Retrograde BMP signaling
642   at the synapse: A permissive signal for synapse maturation and activity-dependent
643   plasticity. *J Neurosci* **33,** 17937-17950.

644 Borst JGG, Helmchen F & Sakmann B. (1995). Pre- and postsynaptic whole-cell recordings in
645   the medial nucleus of the trapezoid body of the rat. *J Physiol* **489,** 825-840.

646 Borst JGG & Soria van Hoeve J. (2012). The calyx of Held synapse: from model synapse to
647   auditory relay. *Annual Review of Physiology* **74,** 199-224.

648 Bosman LWJ, Takechi H, Hartmann J, Eilers J & Konnerth A. (2008). Homosynaptic long-term
649   synaptic potentiation of the "winner" climbing fiber synapse in developing Purkinje
650   cells. *J Neurosci* **28,** 798-807.

651 Carrillo J, Nishiyama N & Nishiyama H. (2013). Dendritic translocation establishes the winner in
652   cerebellar climbing fiber synapse elimination. *J Neurosci* **33,** 7641-7653.

653 Chuhma N & Ohmori H. (1998). Postnatal development of phase-locked high-fidelity synaptic
654   transmission in the medial nucleus of the trapezoid body of the rat. *J Neurosci* **18,** 512-
655   520.

656 Clause A, Kim G, Sonntag M, Weisz CJC, Vetter DE, Rübsamen R & Kandler K. (2014). The
657   precise temporal pattern of prehearing spontaneous activity is necessary for tonotopic
658   map refinement. *Neuron* **82,** 822-835.

659 Colman H, Nabekura J & Lichtman JW. (1997). Alterations in synaptic strength preceding axon
660   withdrawal. *Science* **275,** 356-361.

661 Crins TTH, Rusu SI, Rodríguez-Contreras A & Borst JGG. (2011). Developmental changes in
662   short-term plasticity at the rat calyx of Held synapse. *J Neurosci* **31,** 11706-11717.

663 Darabid H, Perez-Gonzalez AP & Robitaille R. (2014). Neuromuscular synaptogenesis:
664   coordinating partners with multiple functions. *Nat Rev Neurosci* **15,** 703-718.

665 Denk W & Horstmann H. (2004). Serial block-face scanning electron microscopy to reconstruct
666   three-dimensional tissue nanostructure. *PLOS Biology* **2,** e329.

667 Dimitrov D, Takagi H, Guillaud L, Saitoh N, Eguchi K & Takahashi T. (2016). Reconstitution of
668   giant mammalian synapses in culture for molecular functional and imaging studies. *J*
669   *Neurosci* **36,** 3600-3610.

670 Dondzillo A, Sätzler K, Horstmann H, Altrock WD, Gundelfinger ED & Kuner T. (2010). Targeted
671   three-dimensional immunohistochemistry reveals localization of presynaptic proteins
672   Bassoon and Piccolo in the rat calyx of Held before and after the onset of hearing. *J*
673   *Comp Neurol* **518,** 1008-1029.

674 Ehmann H, Hartwich H, Salzig C, Hartmann N, Clément-Ziza M, Ushakov K, Avraham KB,
675   Bininda-Emonds ORP, Hartmann AK, Lang P, Friauf E & Nothwang HG. (2013). Time-
676   dependent gene expression analysis of the developing superior olivary complex. *J Biol*
677   *Chem* **288,** 25865-25879.

678 Fan F, Funk L & Lou X. (2016). Dynamin 1- and 3-mediated endocytosis is essential for the
679   development of a large central synapse *in vivo*. *J Neurosci* **36,** 6097-6115.

680   Felmy F & Schneggenburger R. (2004). Developmental expression of the Ca^{2+}-binding proteins
681   calretinin and parvalbumin at the calyx of Held of rats and mice. *Eur J Neurosci* **20,**
682   1473-1482.

683   Forsythe ID. (1994). Direct patch recording from identified presynaptic terminals mediating
684   glutamatergic EPSCs in the rat CNS, *in vitro*. *J Physiol* **479,** 381-387.

685   Guinan JJ, Jr. & Li RY-S. (1990). Signal processing in brainstem auditory neurons which receive
686   giant endings (calyces of Held) in the medial nucleus of the trapezoid body of the cat.
687   *Hear Res* **49,** 321-334.

688   Gundelfinger ED, Reissner C & Garner CC. (2016). Role of Bassoon and Piccolo in assembly and
689   molecular organization of the active zone. *Frontiers in Synaptic Neuroscience* **7**.

690   Gustafsson MGL. (2005). Nonlinear structured-illumination microscopy: Wide-field
691   fluorescence imaging with theoretically unlimited resolution. *Proceedings of the*
692   *National Academy of Sciences of the United States of America* **102,** 13081-13086.

693   Hamann M, Billups B & Forsythe ID. (2003). Non-calyceal excitatory inputs mediate low fidelity
694   synaptic transmission in rat auditory brainstem slices. *Eur J Neurosci* **18,** 2899-2902.

695   Hamano K, Iwasaki N, Takeya T & Takita H. (1996). A quantitative analysis of rat central
696   nervous system myelination using the immunohistochemical method for MBP. *Dev*
697   *Brain Res* **93,** 18-22.

698   Hashimoto K, Ichikawa R, Kitamura K, Watanabe M & Kano M. (2009). Translocation of a
699   "winner" climbing fiber to the Purkinje cell dendrite and subsequent elimination of
700   "losers" from the soma in developing cerebellum. *Neuron* **63,** 106-118.

701   Hashimoto K & Kano M. (2003). Functional differentiation of multiple climbing fiber inputs
702   during synapse elimination in the developing cerebellum. *Neuron* **38,** 785-796.

703   Held H. (1893). Die centrale Gehörleitung. *Archiv fur Anatomie und Physiologie, Anatomie*
704   *Abtheil*, 201-248.

705   Hoffpauir BK, Grimes JL, Mathers PH & Spirou GA. (2006). Synaptogenesis of the calyx of Held:
706   rapid onset of function and one-to-one morphological innervation. *J Neurosci* **26,**
707   5511-5523.

708   Hoffpauir BK, Kolson DR, Mathers PH & Spirou GA. (2010). Maturation of synaptic partners:
709   functional phenotype and synaptic organization tuned in synchrony. *J Physiol* **588,**
710   4365-4385.

711   Holcomb PS, Hoffpauir BK, Hoyson MC, Jackson DR, Deerinck TJ, Marrs GS, Dehoff M, Wu J,
712   Ellisman MH & Spirou GA. (2013). Synaptic inputs compete during rapid formation of
713   the calyx of Held: a new model system for neural development. *J Neurosci* **33,** 12954-
714   12969.

715   Hsieh CY, Nakamura PA, Luk SO, Miko IJ, Henkemeyer M & Cramer KS. (2010). Ephrin-B reverse
716   signaling is required for formation of strictly contralateral auditory brainstem
717   pathways. *J Neurosci* **30,** 9840-9849.

718   Kandler K & Friauf E. (1993). Pre- and postnatal development of efferent connections of the
719   cochlear nucleus in the rat. *Journal of Comparative Neurology* **328,** 161-184.

720   Körber C, Dondzillo A, Eisenhardt G, Herrmannsdörfer F, Wafzig O & Kuner T. (2014). Gene
721   expression profile during functional maturation of a central mammalian synapse. *Eur J*
722   *Neurosci* **40,** 2867-2877.

723   Kronander E, Clark C & Schneggenburger R. (2019). Role of BMP signaling for the formation of
724   auditory brainstem nuclei and large auditory relay synapses. *Developmental*
725   *Neurobiology* **79,** 155-174.

726   Kuwabara N, DiCaprio RA & Zook JM. (1991). Afferents to the medial nucleus of the trapezoid
727   body and their collateral projections. *Journal of Comparative Neurology* **314,** 684-706.

728   Liang L, Fratzl A, Goldey G, Ramesh RN, Sugden AU, Morgan JL, Chen C & Andermann ML.
729   (2018). A fine-scale functional logic to convergence from retina to thalamus. *Cell* **173,**
730   1343-1355 e1324.

731 Lohmann C & Friauf E. (1996). Distribution of the calcium-binding proteins parvalbumin and
732   calretinin in the auditory brainstem of adult and developing rats. *J Comp Neurol* **367,**
733   90-109.
734 Lorteije JAM, Rusu SI, Kushmerick C & Borst JGG. (2009). Reliability and precision of the mouse
735   calyx of Held synapse. *J Neurosci* **29,** 13770-13784.
736 Marrs GS & Spirou GA. (2012). Embryonic assembly of auditory circuits: spiral ganglion and
737   brainstem. *J Physiol* **590,** 2391-2408.
738 Matho KSH. (2013). Structure and dynamism in a central neural circuit in adulthood and
739   postnatal development. In *École Doctorale Cerveau, Cognition, Comportement*.
740   Université Pierre et Marie Curie, Paris, France.
741 Michalski N, Babai N, Renier N, Perkel DJ, Chédotal A & Schneggenburger R. (2013). Robo3-
742   driven axon midline crossing conditions functional maturation of a large commissural
743   synapse. *Neuron* **78,** 855-868.
744 Milinkeviciute G, Henningfield CM, Muniak MA, Chokr SM, Green KN & Cramer KS. (2019).
745   Microglia regulate pruning of specialized synapses in the auditory brainstem. *Frontiers*
746   *in Neural Circuits* **13**.
747 Morest DK. (1968). The growth of synaptic endings in the mammalian brain: a study of the
748   calyces of the trapezoid body. *Zeitschrift für Anatomie und Entwicklungsgeschichte*
749   **127,** 201-220.
750 Nakamura PA & Cramer KS. (2011). Formation and maturation of the calyx of Held. *Hear Res*
751   **276,** 70-78.
752 Nothwang HG, Ebbers L, Schlüter T & Willaredt MA. (2015). The emerging framework of
753   mammalian auditory hindbrain development. *Cell Tissue Res* **361,** 33-48.
754 Qiu X, Zhu Q & Sun J. (2015). Quantitative analysis of vesicle recycling at the calyx of Held
755   synapse. *Proceedings of the National Academy of Sciences* **112,** 4779-4784.
756 Rodríguez-Contreras A, de Lange RPJ, Lucassen PJ & Borst JGG. (2006). Branching of calyceal
757   afferents during postnatal development in the rat auditory brainstem. *J Comp Neurol*
758   **496,** 214-228.
759 Rodríguez-Contreras A, van Hoeve JS, Habets RLP, Locher H & Borst JGG. (2008). Dynamic
760   development of the calyx of Held synapse. *Proc Natl Acad Sci U S A* **105,** 5603-5608.
761 Rollenhagen A & Lübke JHR. (2006). The morphology of excitatory central synapses: from
762   structure to function. *Cell Tissue Res* **326,** 221-237.
763 Rozeik C & Von Keyserlingk D. (1987). The sequence of myelination in the brainstem of the rat
764   monitored by myelin basic protein immunohistochemistry. *Developmental Brain*
765   *Research* **35,** 183-190.
766 Rusu SI & Borst JGG. (2011). Developmental changes in intrinsic excitability of principal
767   neurons in the rat medial nucleus of the trapezoid body. *Dev Neurobiol* **71,** 284-295.
768 Sanes JR & Lichtman JW. (1999). Development of the vertebrate neuromuscular junction. *Annu*
769   *Rev Neurosci* **22,** 389-442.
770 Sätzler K, Söhl LF, Bollmann JH, Borst JGG, Frotscher M, Sakmann B & Lübke JHR. (2002). Three-
771   dimensional reconstruction of a calyx of Held and its postsynaptic principal neuron in
772   the medial nucleus of the trapezoid body. *J Neurosci* **22,** 10567-10579.
773 Savtchenko LP. (2007). Bilateral processing in chemical synapses with electrical 'ephaptic'
774   feedback: a theoretical model. *Math Biosci* **207,** 113-137.
775 Schindelin J, Arganda-Carreras I, Frise E, Kaynig V, Longair M, Pietzsch T, Preibisch S, Rueden C,
776   Saalfeld S, Schmid B, Tinevez JY, White DJ, Hartenstein V, Eliceiri K, Tomancak P &
777   Cardona A. (2012). Fiji: an open-source platform for biological-image analysis. *Nat*
778   *Methods* **9,** 676-682.
779 Schneggenburger R & Forsythe ID. (2006). The calyx of Held. *Cell Tissue Res* **326,** 311-337.
780 Schneider CA, Rasband WS & Eliceiri KW. (2012). NIH Image to ImageJ: 25 years of image
781   analysis. *Nat Methods* **9,** 671-675.

782 Sierksma MC & Borst JGG. (2017). Resistance to action potential depression of a rat axon terminal in vivo. *Proc Natl Acad Sci U S A* **114,** 4249-4254.

784 Sierksma MC, Tedja MS & Borst JGG. (2016). *In vivo* matching of postsynaptic excitability with spontaneous synaptic inputs during formation of the rat calyx of Held synapse. *J Physiol* **595,** 207-231.

787 Sommer I, Lingenhöhl K & Friauf E. (1993). Principal cells of the rat medial nucleus of the trapezoid body: an intracellular in vivo study of their physiology and morphology. *Experimental Brain Research* **95,** 223-239.

790 Sonntag M, Englitz B, Kopp-Scheinpflug C & Rübsamen R. (2009). Early postnatal development of spontaneous and acoustically evoked discharge activity of principal cells of the medial nucleus of the trapezoid body: an *in vivo* study in mice. *J Neurosci* **29,** 9510-9520.

794 Soria Van Hoeve J & Borst JGG. (2010). Delayed appearance of the scaffolding proteins PSD-95 and Homer-1 at the developing rat calyx of Held synapse. *J Comp Neurol* **518,** 4581-4590.

797 Spirou GA, Chirila FV, von Gersdorff H & Manis PB. (2008). Heterogeneous Ca^{2+} influx along the adult calyx of Held: a structural and computational study. *Neuroscience* **154,** 171-185.

799 Südhof Thomas C. (2012). The presynaptic active zone. *Neuron* **75,** 11-25.

800 Taschenberger H, Leão RM, Rowland KC, Spirou GA & von Gersdorff H. (2002). Optimizing synaptic architecture and efficiency for high-frequency transmission. *Neuron* **36,** 1127-1143.

803 Taschenberger H & von Gersdorff H. (2000). Fine-tuning an auditory synapse for speed and fidelity: developmental changes in presynaptic waveform, EPSC kinetics, and synaptic plasticity. *J Neurosci* **20,** 9162-9173.

806 Tritsch NX, Rodríguez-Contreras A, Crins TTH, Wang HC, Borst JGG & Bergles DE. (2010). Calcium action potentials in hair cells pattern auditory neuron activity before hearing onset. *Nat Neurosci* **13,** 1050-1052.

809 Walmsley B, Alvarez FJ & Fyffe REW. (1998). Diversity of structure and function at mammalian central synapses. *Trends in Neurosciences* **21,** 81-88.

811 Wang T, van Woerden GM, Elgersma Y & Borst JGG. (2017). Enhanced transmission at the calyx of Held synapse in a mouse model for Angelman syndrome. *Front Cell Neurosci* **11,** 418.

814 Watanabe M & Kano M. (2011). Climbing fiber synapse elimination in cerebellar Purkinje cells. *Eur J Neurosci* **34,** 1697-1710.

816 Willaredt MA, Schlüter T & Nothwang HG. (2015). The gene regulatory networks underlying formation of the auditory hindbrain. *Cell Mol Life Sci* **72,** 519-535.

818 Wimmer VC, Nevian T & Kuner T. (2004). Targeted in vivo expression of proteins in the calyx of Held. *Pflügers Arch* **449,** 319-333.

820 Winnubst J, Cheyne JE, Niculescu D & Lohmann C. (2015). Spontaneous activity drives local synaptic plasticity in vivo. *Neuron* **87,** 399-410.

822 Xiao L, Michalski N, Kronander E, Gjoni E, Genoud C, Knott G & Schneggenburger R. (2013). BMP signaling specifies the development of a large and fast CNS synapse. *Nat Neurosci* **16,** 856-864.

825 Yu WM & Goodrich LV. (2014). Morphological and physiological development of auditory synapses. *Hear Res* **311,** 3-16.

827

828

829 **Additional information**

830 **Competing interests**: The authors declare no competing financial interests.

831 **Contributions**

832 JGGB and MCS designed experiments. MCS performed *in vivo* electrophysiology and imaging

833 experiments, analyzed the electrophysiology and the images. JAS performed imaging

834 experiments and imaging analysis. ABH, JAS and JGGB designed imaging analysis. MCS drafted

835 the manuscript. JAS, ABH and JGGB revised it critically for important intellectual content. All

836 authors approved the final version of the manuscript and agree to be accountable for all

837 aspects of the work in ensuring that questions related to the accuracy or integrity of any part

838 of the work are appropriately investigated and resolved. All persons designated as authors

839 qualify for authorship, and all those who qualify for authorship are listed.

845

846   *Figure list*

847   **Figure 1. Responses to current stimulation of developing calycigenic axons.**

848   **Figure 2. Synaptic competition in MNTB follows the expansion of the strongest input without**

849   **changing the second strongest input.**

850   **Figure 3. Comparison of strong inputs with and without prespikes.**

851   **Figure 4. Developmental expression of Piccolo in the MNTB.**

852   **Figure 5. Contact area of perisomatic VGluT clusters correlates with synaptic strength *in vivo***
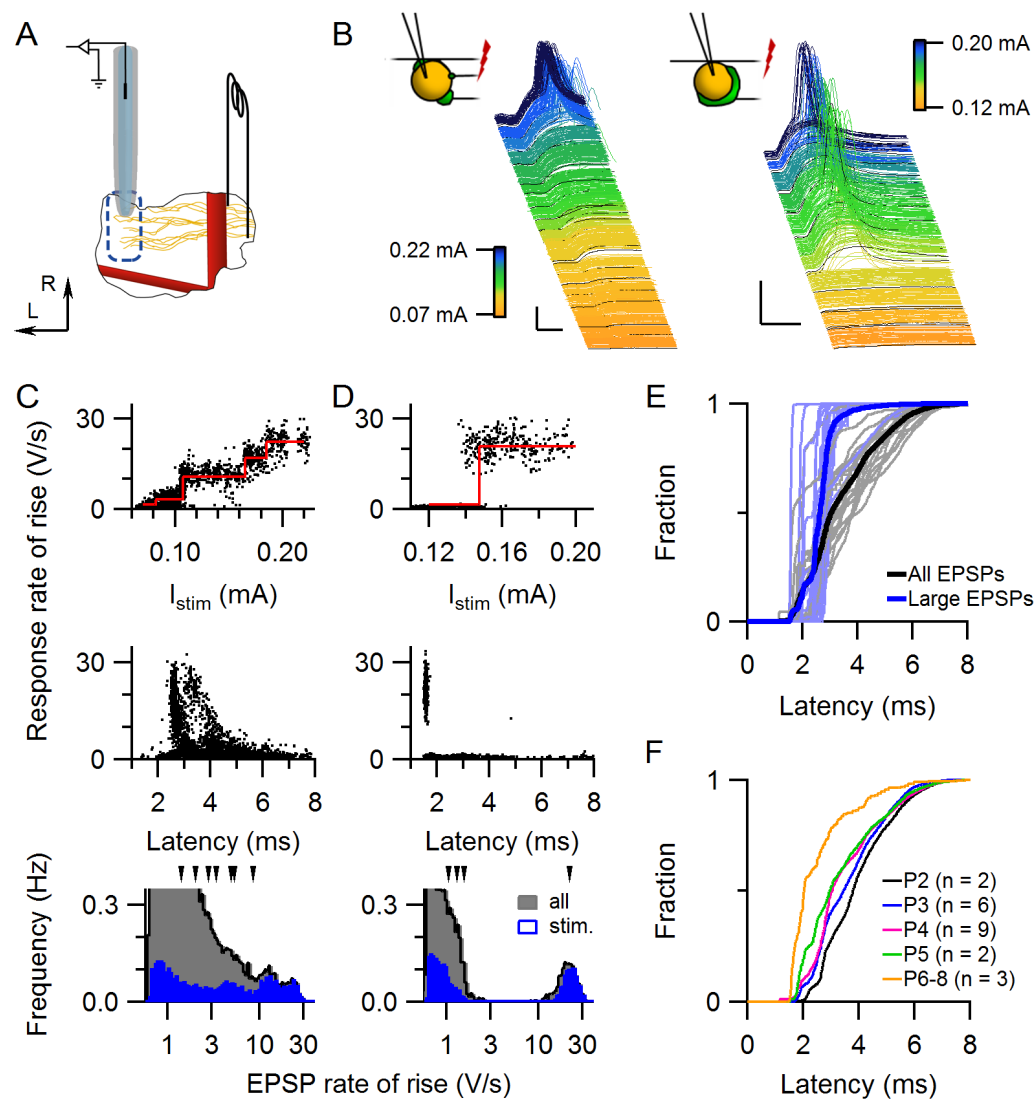
Figure 1. Responses to current stimulation of developing calycigenic axons. (A) Schematic

drawing of the experimental approach. A bipolar stimulation electrode straddling the

trapezoid body was positioned contralaterally from the recorded MNTB, and whole-cell

recordings were made from principal cells of the MNTB. The basilar artery (rostrocaudal, thick

red line) and the anterior-inferior cerebellar artery (mediolateral, red line) served as

landmarks. Arrows indicate lateral (L) and rostral (R) directions. (B) Waterfall plots of two

whole-cell recordings, sorted on stimulation intensity (color-coded as indicated in calibration

bars). In the P4 example (left) a gradual increase in the evoked EPSP was observed, suggesting

the recruitment of multiple inputs, while in the P6 example (right) a single, large EPSP was

862   observed, which elicited a postsynaptic AP. Schematic drawing depicts the assumed synaptic

863   innervation. Scale bars indicate 25 mV and 2 ms. (C) Identification of synaptic inputs. Rates of

864   rise of evoked EPSPs vs. stimulation intensity (top) or EPSP latency (middle) for the P4 example

865   shown in B. The bottom graph shows the histograms of the rates of rise of evoked and

866   spontaneous EPSPs. Arrow heads on top of the graph indicate the rates of rise of identified

867   inputs. Data points in the top graph were horizontally scattered by <50 µA for visualization

868   purposes. (D) As C, except for the P6 example shown in B. (E) Cumulative distribution of

869   latencies of all evoked EPSPs (black) and of large EPSPs (>10 V/s, blue). Individual cells are

870   shown in light blue and grey. Large EPSPs have a shorter latency than most other EPSPs. (F)

871   The average cumulative distribution of the evoked EPSP latencies grouped by age suggests a

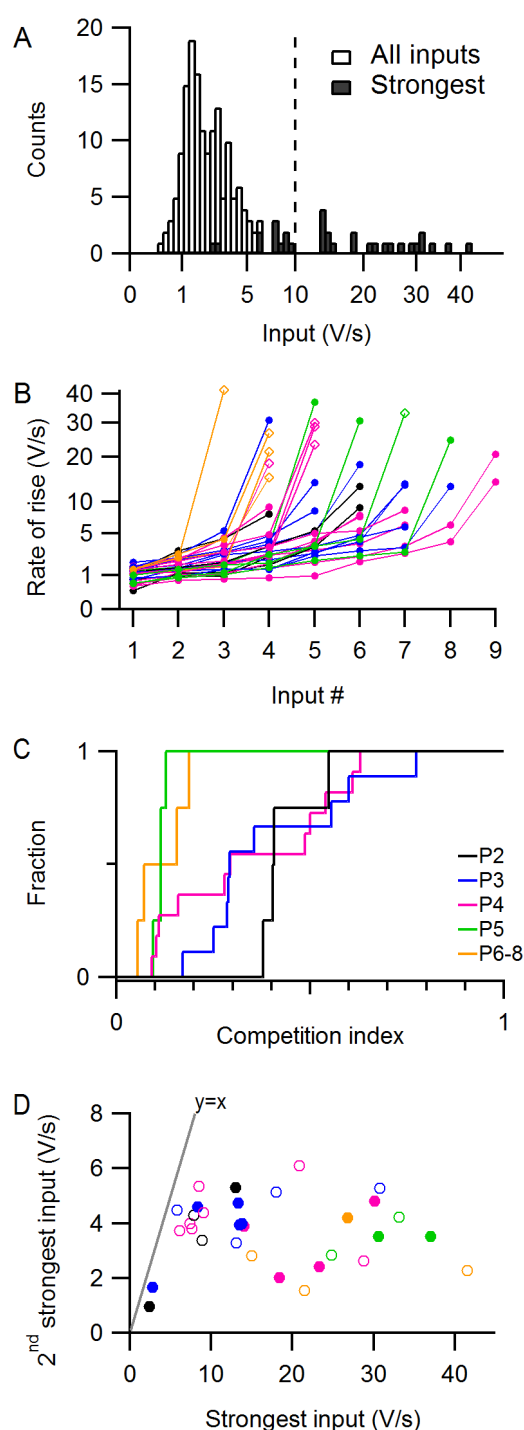872   developmental increase in propagation speed.

Figure 2. Synaptic competition in MNTB follows the expansion of the strongest input without changing the second strongest input. (A) Histogram of the average rate of rise for all inputs (open) and the strongest inputs (closed). Line indicates the threshold for 'strong inputs'. (B) For every cell the inputs are incrementally sorted by their average EPSP rate of rise. Diamonds

36

877   indicate the inputs associated with a prespike. Colors indicate the ages as in C. Note the root

878   scale of the ordinate. (C) Cumulative distributions of the competition index, i.e. the ratio of the

879   rates of rise of the second strongest to the strongest input. (D) The rate of rise of the second

880   strongest input against the strongest. Markers correspond to individual principal cells. Closed

881   markers indicate that both inputs were identified based on spontaneous activity. Line shows

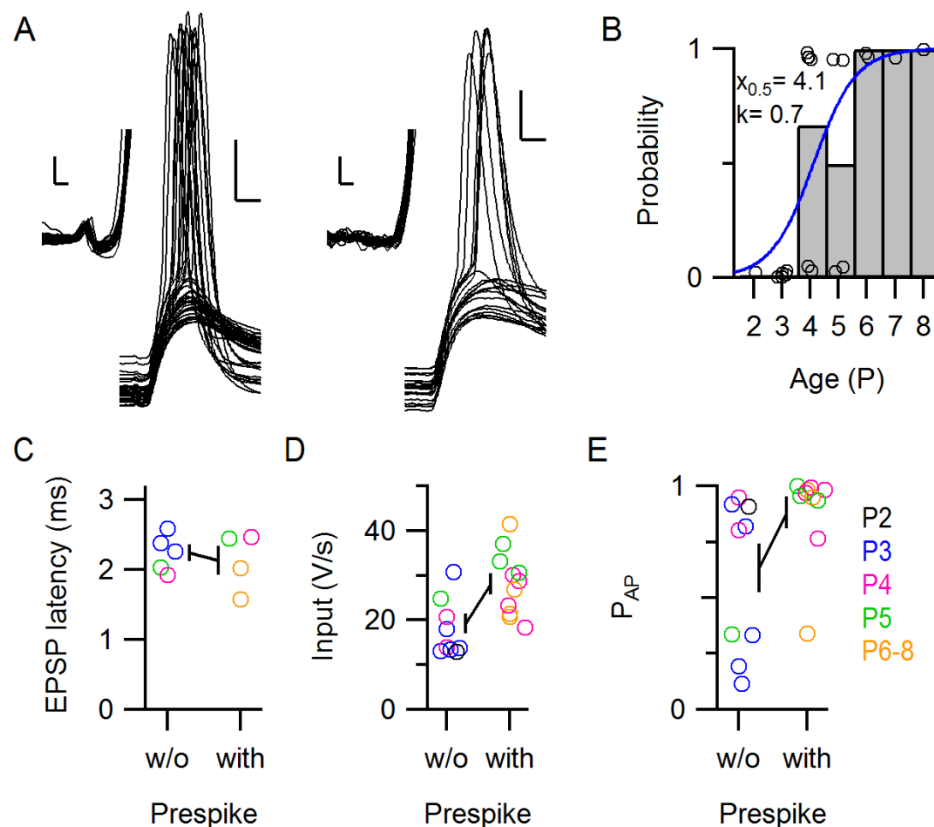882   identity line. Colors indicate age as in C.

883   **Figure 3. Comparison of strong inputs with and without prespikes.** (A) Large EPSPs of a strong

884   input with (left; P6) and of a strong input without (right; P5) a prespike. EPSPs were aligned on

885   their onset. The insets show the same traces with their V_m offsets subtracted. Scale bars

886   indicate 10 mV and 1 ms, and scale bars in the inset indicate 0.5 mV and 0.2 ms. (B)

887   Developmental changes in the presence of a prespike preceding a large EPSP. Circles indicate

888   cells where a large EPSP was recorded. Bars represent age average. Blue line represents the fit

889   of the logistic function with the values reported in the graph. (C-E) Comparison of EPSP

890   latency, average EPSP rate of rise and probability of eliciting postsynaptic APs (P_{AP}) for strong

891   inputs with or without a prespike. In C only evoked large EPSPs were analyzed. Circles indicate

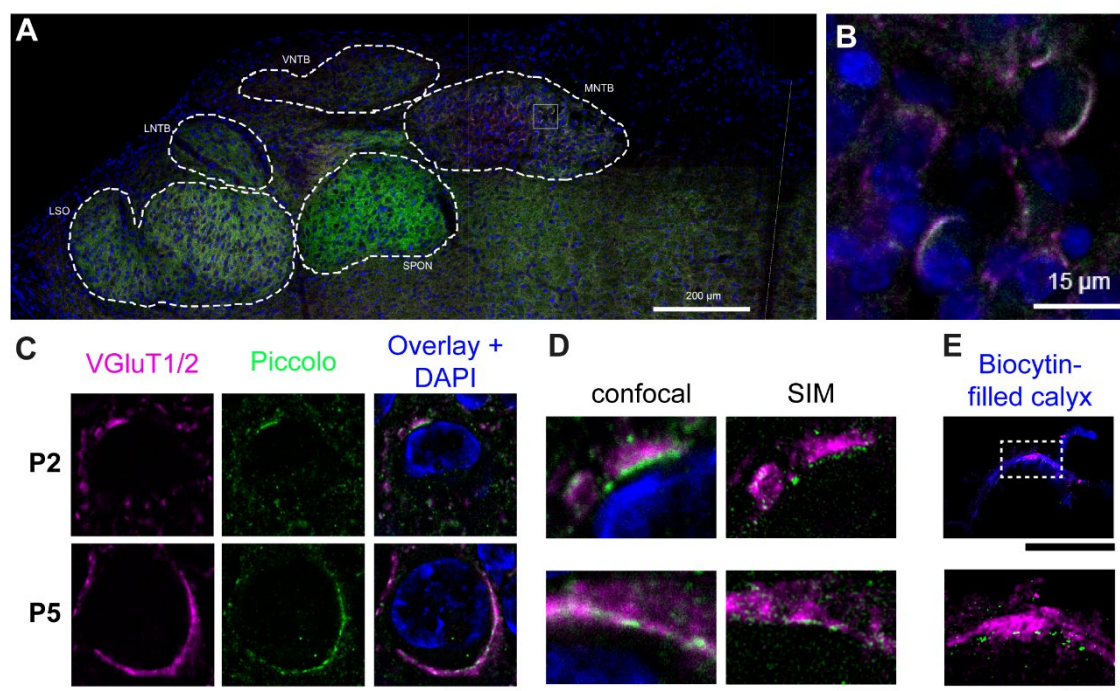892   individual cells. Line represents the average and SEM.

893

Figure 4. Developmental expression of Piccolo in the MNTB. (A) Fluorescent labeling of

Piccolo (green), VGluT (magenta) and DAPI (blue) in the SOC of a P4 rat. Midline is indicated

with a white line. Auditory nuclei are delineated with dashed lines. (B) Higher magnification of

the grey box in A showing principal cells of the MNTB with large perisomatic clusters of VGluT

and Piccolo. (C) A P2 and P5 principal cell with fluorescent labeling of VGluT, Piccolo, and

VGluT + Piccolo + DAPI with confocal microscopy. (D) Comparison of confocal microscopy and

SIM of perisomatic clusters of Piccolo and VGluT of the P2 principal cell shown in C (top), and

of the P5 principal cell shown in C (bottom). (E) SIM image of a P5 biocytin-filled calyx (top,

blue) with VGluT and Piccolo, revealing active zone-like structures in the Piccolo labeling

(bottom). Non-calyceal labeling was masked. Scale bars indicate 200 µm in A, 15 µm in B, 10

µm in C, 2 µm in D, and 10 and 1 µm in E. Images in C and D were background-subtracted.

Abbreviations: LSO, lateral superior olive; MNTB, medial nucleus of the trapezoid body; P,

postnatal; SIM, structured-illumination microscopy; SOC, superior olivary complex; SPON,

superior periolivary nucleus; VGluT, vesicular glutamate transporter 1 and 2; VNTB, ventral
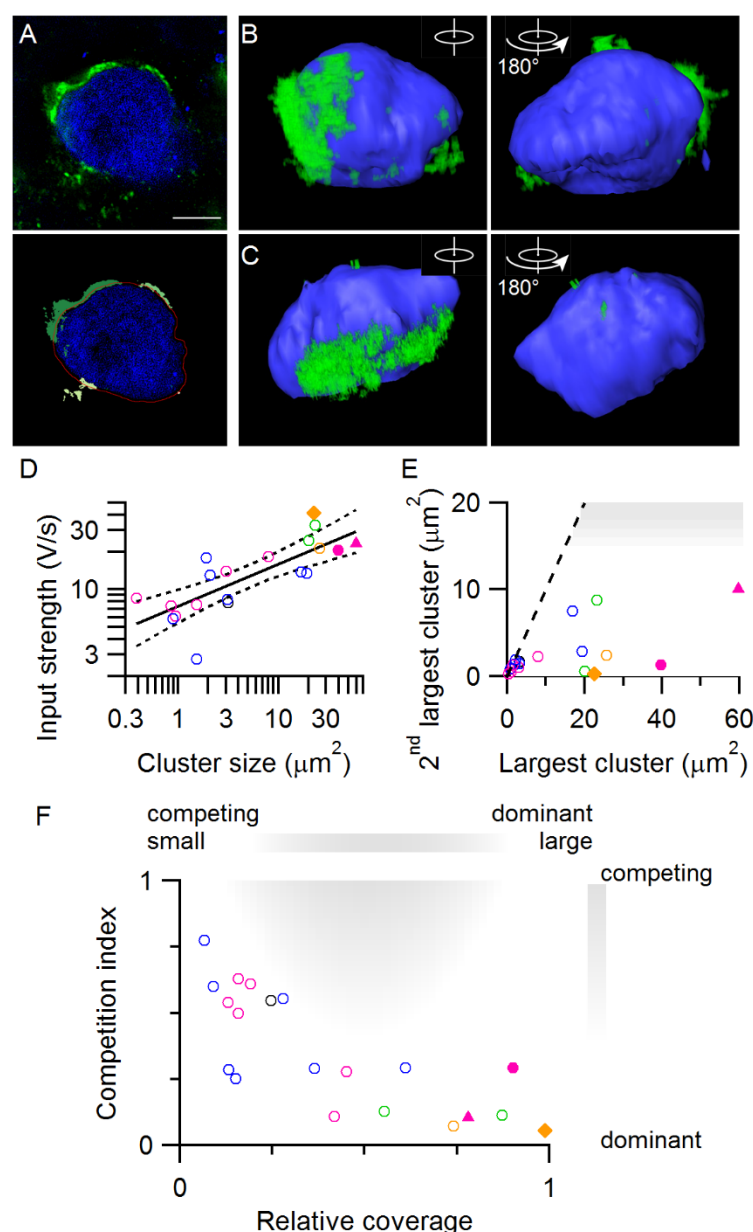
nucleus of the trapezoid body.

39

909 **Figure 5. Contact area of perisomatic VGluT clusters correlates with synaptic strength *in vivo*.**

910 (A) Example of segmentation of VGluT clusters around the soma. The image before (top) and

911 after segmentation (below). Blue: biocytin; Green: VGluT labeling. In the bottom image

912 different VGluT clusters are depicted by different shades of green. Red line indicates contour

913 of the cell after dilation. For this cell 1 input was associated with a prespike. (B-C) 3D

914 reconstructions of somata (blue) with VGluT clusters (green). Dendrites were manually

915   removed. Right image is the same soma after 180 degrees rotation. Postsynaptic cell in B did

916   not have a prespike-associated input. The VGluT cluster in C was manually separated from a

917   nearby cluster that terminated on another cell. (D) Relation between input strength of

918   strongest input and contact area of the largest VGluT cluster for each cell. Line indicates linear

919   fit of log-transformed variables. Dotted line indicates 95% confidence intervals. (E) Relation

920   between area of largest and second largest VGluT cluster. Shaded area: possibly multi-calyceal

921   innervation. (F) Competition index against relative coverage. Competition index equals the

922   second strongest input relative to the strongest input. Relative coverage equals the contact

923   area of the largest VGluT cluster relative to the total area contacted by VGluT clusters. Shaded

924   area indicates region where data points with multi-calyceal competition are expected to

925   appear. Colors in D-G indicate age as in previous figures. Triangle indicates the data point that

926   corresponds to the cell shown in A. Closed circle and diamond indicate data points

927   corresponding to the cells shown in B and C, respectively.